

Enhancing the photomixing efficiency of optoelectronic devices in the terahertz regime

Subrahmanyam Pilla

Department of Physics, University of California, San Diego, CA 92093*

A method to reduce the transit time of majority of carriers in photomixers and photo detectors to < 1 ps is proposed. Enhanced optical fields associated with surface plasmon polaritons, coupled with velocity overshoot phenomenon results in net decrease of transit time of carriers. As an example, model calculations demonstrating $> 280\times$ (or ~ 2800 and $31.8 \mu\text{W}$ at 1 and 5 THz respectively) improvement in THz power generation efficiency of a photomixer based on Low Temperature grown GaAs are presented. Due to minimal dependence on the carrier recombination time, it is anticipated that the proposed method paves the way for enhancing the speed and efficiency of photomixers and detectors covering UV to far infrared communications wavelengths (300 to 1600 nm).

Recent experimental observation of extraordinary optical transmission through a normal metal film having subwavelength holes[1] has generated intense interest in harnessing the underlying physics for photonic applications. It is widely believed that quasi two-dimensional electromagnetic excitations tightly bound to the metal surface known as Surface Plasmon Polaritons (SPPs) are responsible for the observed near field enhancement of the optical radiation. Exponential decay of field components arising from SPPs (penetrating ~ 100 , ~ 10 nm in dielectric and metal respectively), make them highly attractive for miniature photonic circuits and devices[2]. Currently, several potential applications of SPPs are being explored including wave guiding[3] and near-field microscopy[4]. However, application of SPPs to enhance the speed and efficiency of photo detectors or photomixers has not been attempted due to the complexity of underlying physics and optimal device designs involving complicated dielectric-metal structures.

In this letter we propose a simple interdigitated metal structure embedded in a suitable semiconductor material to harness SPPs for improving the speed and efficiency of photomixers and detectors. Such a device can be realized with the existing material growth techniques[5]. As an example, we demonstrate via model calculations, significant ($> 280\times$) improvement in the efficiency of a THz photomixer based on Low Temperature grown GaAs (LT-GaAs). Microwave to THz radiation sources in the 0.1 to 10 THz are being extensively studied for their application in communications, medical imaging, and spectroscopy[6, 7, 8, 9, 10]. For many applications- compact, narrow-linewidth, widely tunable continuous wave sources are necessary. In particular, to be used as a local oscillator in communications systems the THz source should produce stable output power $> 10 \mu\text{W}$ [8, 11]. Among the various techniques being pursued[6, 8, 11, 12, 13] electrical down conversion of optical microwave sources in a suitable photomixer[6, 11, 12] are appealing due to the easy availability of tunable, narrow-linewidth, and stable solid state lasers. However, until now the output power from these photomixers is limited to $< 10 \mu\text{W}$ in the cru-

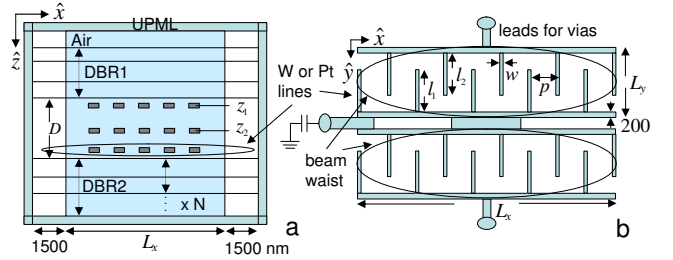


FIG. 1: Schematic of FP cavity (a) and a layer of interdigitated metal lines (b) modelled using FDTD and FD simulators. The FP cavity is formed by 3 or 4 dielectric layers constituting DBR₁, N pairs of low/high refractive index dielectric layers constituting DBR₂, and absorbing layer of thickness D . The active volume is terminated by 15 cell UPML layers in FDTD implementation. The lines parallel to the x axis (width 200 nm) are connected to either signal transmission lines or planar antenna fabricated on top of the absorbing layer (not shown). Through layer vias electrically connect identical layers of interdigitated lines (b) placed at various depths z_i within the absorbing layer. The overall dimensions of the absorbing volume (excluding DBRs and via leads) are given by L_x , L_y , D whereas number of interdigitated metal layers, their vertical positions, (measured from the Air-DBR₁ interface), the metal line (finger) thickness, pitch, width, and lengths of +ve and -ve electrodes are given by i , z_i , d , p , w , l_1 , l_2 as shown. $x = 0$, $y = 0$ is located at the center of top half of the interdigitated pattern in (b). When the top and bottom interdigitated structures in (b) are connected in series as shown with the center electrode grounded, the resulting structure can be excited by lasers forming two quasi-elliptical spots. Such a radiation pattern is achievable by choosing proper laser propagation mode (such as TEM₀₁ mode). The spacing between the two halves is adjusted to match the beam pattern of the specific laser system being used.

cial THz range. In a conventional Metal-Semiconductor-Metal (MSM) photomixer[14], optically thick (100 nm) interdigitated metal lines are fabricated on a high resistivity semiconductor with subpicosecond recombination time of carriers (τ_e/τ_h for electrons/holes respectively) and high breakdown field limit. So far, only a few materials such as LT-GaAs[6, 14] and Fe implanted InGaAs[15]

have been shown to meet these requirements. From the photomixer theory, when two lasers (wavelengths λ_1, λ_2 , $\lambda_0 = (\lambda_1 + \lambda_2)/2$, and powers $P_1 = P_2 = P_0/2$) with their difference frequency $f = c(\lambda_1^{-1} - \lambda_2^{-1})$ in the THz range are incident on a dc biased photomixer[14], the THz wave output power P_f is given by

$$P_f = \frac{\frac{1}{2}R_L i_p^2}{[1 + (2\pi f(R_L + R_S)C)^2]}, \quad (1)$$

where i_p is the photocurrent generated in the external circuit, c is velocity of light in free space, C is the capacitance, R_S is small internal resistance of the metal structure, and R_L is the load resistance in the 72-200 range[6, 12, 14]. To accelerate carriers generated deep inside the semiconductor, high dc voltage ($V_b \approx 40$ V) is applied across the electrodes. This results in fields quickly exceeding the breakdown limit near the electrodes leading to device failure. As the carrier transport is transit time (t_{tr}) limited, i. e., $t_{tr} > f^{-1}$, recombination time $\tau \ll f^{-1}$ is required to recombine the carriers that do not contribute to i_p before the beat cycle reverses[12, 14]. Even if the photomixer is placed in a suitable optical cavity, due to strong reflection from thick metal electrodes, no carriers are generated directly below the electrodes where t_{tr} will be small. In addition, subwavelength features of the metal lines produce strong near field diffraction patterns that are not taken into account in conventional designs[6, 12, 14].

In the present technique, we exploit SPPs for generating more carriers close to subwavelength normal metal electrodes embedded in a photoconductor layer sandwiched between two Distributed Bragg Reflectors (DBR) that form a Fabry-Perot (FP) cavity. When coupled with velocity overshoot phenomenon reported in many photoconductor materials[12, 16, 17, 18, 19, 20], t_{tr} of majority of carriers is reduced to < 1 ps, i.e., $t_{tr} \leq f^{-1}$. For efficient use of SPPs, it is desirable to have thin (~ 10 nm) normal metal lines with subwavelength features distributed throughout the active volume (Fig 1a) in a manner that would collectively enhance the optical field intensity in the vicinity of the metal lines. This must however be accomplished without significantly increasing C and R_S . We show that for the proposed structure (Fig 1) optimized for $\lambda_0 = 850$ nm, P_f is ~ 2800 and $31.8 \mu\text{W}$ at $f = 1$ and 5 THz respectively. A convenient way to model such a complex structure is to solve the Maxwell's equations with appropriate boundary conditions using Finite Difference Time-Domain (FDTD) formulation[22, 23, 27]. A 3D-FDTD simulator with Uniaxial Perfectly Matched Layer (UPML)[23] surrounding the photomixer is developed for this purpose. Along the z -axis, the active volume consists of a few hundred nm of free space followed by DBR₁, absorbing region with complex structure of normal metal electrodes, and pairs of low/high refractive index layers constituting DBR₂ (Fig

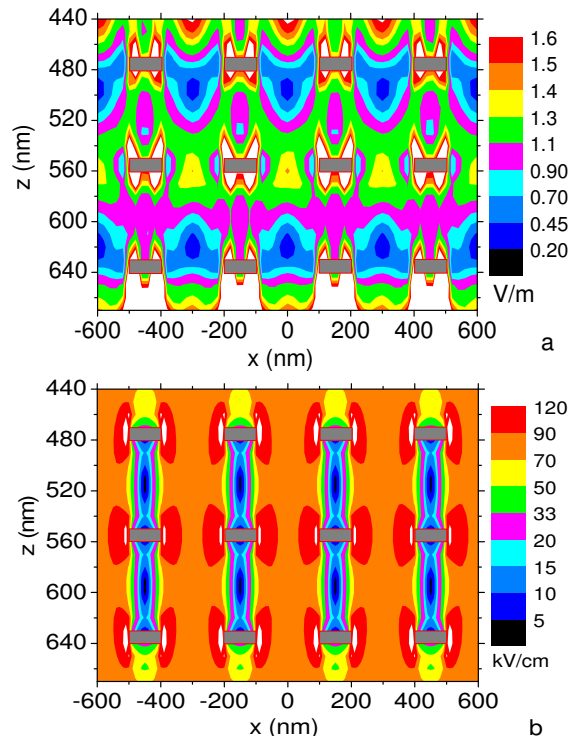


FIG. 2: Optical electric field amplitude (a) and dc electric field strength (b) inside the $D = 230$ nm LT-GaAs absorbing layer of the photomixer design of Fig 1 optimized for $\lambda_0 = 850$ nm. Incident optical field amplitude $E_x^0 = 1$ V/m and $V_b = \pm 1$ V. For clarity, fields in only the $x = \pm 600$ nm region along the $y = 0$ plane are plotted. The grey rectangular regions in the plots show the cross-section of the interdigitated W lines with $L_x = 7000$, $L_y = 2500$, $d = 10$, $z_1 = 475$, $z_2 = 555$, $z_3 = 635$, $p = 300$, $w = 100$, $l_1 = 1500$, $l_2 = 1400$ nm respectively. $C = 4.90$ fF and $R_S = 2.4 \Omega$ for this device. The FP cavity is formed by three layers of (TiO_2 , Si_3N_x , CaF_2) constituting DBR₁ (refractive indices (2.4, 2.0, 1.23 to 1.36)[25] and thicknesses (100, 150, 190) nm for each layer respectively), four pairs of (Al_2O_x , GaAs) layers[24] forming DBR₂ (refractive indices (1.6, $3.53 - 0.068i$) and thicknesses (130, 60) nm), and $D \approx \lambda$ absorbing LT-GaAs layer with refractive index $3.77 - 0.068i$.

1a)[24]. For a given D , the refractive index and thickness of DBR layers are first optimized by calculating the reflection and transmission coefficients of the FP cavity using matrix methods[25]. The FP cavity is excited by a linearly polarized, plane wave propagating along $+z$ direction, with gaussian (elliptic) intensity profile in the $x - y$ plane. The source plane is placed in the free space above the DBR₁. Frequency-domain Lorentz dispersion model[26] is adapted for metals with negative dielectric constant such as W or Pt.

Figure 2a shows the FDTD results of a three layer stack of interdigitated W lines embedded in 230 nm LT-GaAs absorbing layer of a photomixer design of Fig 1 optimized for $\lambda_0 = 850$ nm. The plot clearly shows the

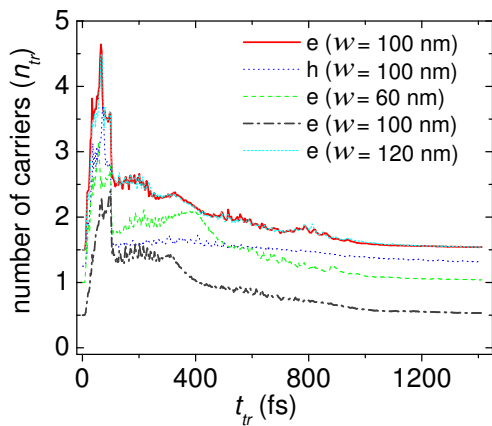


FIG. 3: Carrier transit time distribution $n_{tr}(t_{tr})$ for electrons (e) and holes (h) in the photomixer design of Fig 1. The parameters for red (solid) and blue (dot) curves are same as in Fig 2 with $w = 100$ nm where as for grey (dash-dot) curve only polarization is changed to E_y . For the green (dash) and cyan (short dash) curves (L_x, p, w) are changed to (7560, 300, 60) and (7480, 320, 120) nm respectively while rest of the parameters remaining unaltered from those of Fig 2. The photomixer is excited by an 850 nm source at $P_0 = 60$ mW for all structures. For clarity, the curves are shifted along y -axis and the relative shift can be easily obtained from the values at $t_{tr} = 0$ fs.

near field enhancement resulting from the thin normal metal electrodes. In the absence of the W electrodes, we obtain electric field amplitude maxima (maximum amplitude 1.4 V/m) corresponding to three antinodes in the standing wave formed between the DBRs. The 3D internal dc electric fields and C are computed by solving Laplace's equation with appropriate boundary conditions using FD techniques[27]. Figure 2b shows the contour plot of the static electric field strength within the LT-GaAs layer. The data show that unlike the traditional MSM structure, the field strength in this design is well above the critical field (~ 5 kV/cm). Moreover, the field strength is ~ 90 kV/cm between neighboring electrodes, in particular at the center of the device where most of the carriers are generated due to gaussian intensity profile of the incident laser beams. In the rest of the volume it has a broad peak at 18 kV/cm (not shown). Results show that $C = 4.90$ fF and $R_S = 2.4 \Omega$ based on the resistivity of thin annealed or epitaxial W films ($\sim 5 \mu\Omega\text{-cm}$)[28]. The highest electric field inside the device is about four times lower than the breakdown field (500 kV/cm); therefore device failure due to electric breakdown is unlikely for this $V_b = \pm 1$ V.

Photocurrent i_p is calculated by first computing the electron/hole transit time distributions $n_{tr}^e(t_{tr})$, $n_{tr}^h(t_{tr})$ shown in Fig 3 for the entire absorbing volume based on the above FDTD and FD calculations. From the data available in literature for GaAs and LT-GaAs, for

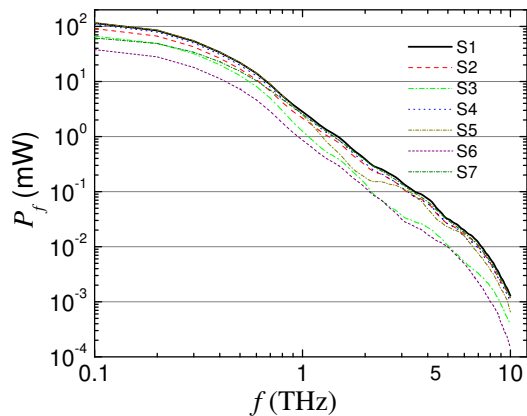


FIG. 4: Calculated THz output power P_f from the photomixer design of Fig 1 excited by $\lambda_0 = 850$ nm radiation with incident power $P_0 = 60$ mW. $\tau = 4$ ps for designs S1 to S6 where as for S7 $\tau = 1$ ps. Parameters for S1 are same as in Fig 2 whereas for S2 $z_3 = 645$ nm, for S3 $z_3 = 645$ nm and incident radiation is E_y polarized, for S4 (p, w) are (320, 120) nm respectively, for S5 (L_x, w) are (7560, 60) nm respectively, and for S6 (z_1, z_3) are (455, 655) nm respectively. The remaining unlisted parameters are the same in all cases. In all designs the interdigitated lines in different layers have no relative orientation angle differences.

$t_{tr} \leq t_{onset} = 100$ fs, the carrier motion can be approximated by ballistic transport with electron effective mass $m_e = 0.088m_0$, where m_0 is electron rest mass. This value is consistent with the slope of the linear portion of transient drift velocity curve obtained from Monte-Carlo calculations[18]. The corresponding effective mass for holes is $m_h = 0.106m_0$. Effective masses larger than the accepted values for GaAs (0.063, 0.076 m_0 for electron and light holes respectively) are considered so that longer t_{tr} , thereby lower estimate of i_p results from these calculations. In the photomixer of Fig 2, pure ballistic transport is applicable to electrons generated close to the +ve electrodes and holes generated close to -ve electrodes. These carriers generated predominantly in the near field enhancement region, transit through non-uniform dc fields in the 5 to 90 kV/cm range. It should be noted that $t_{onset} = 100$ fs is considerably lower than the theoretical limit of ballistic motion in GaAs for this field strength range[16]. For $t_{tr} \geq t_{onset}$, electron motion is approximated by qasiballistic transport with time dependent velocity distribution similar to ref. 18 up to $t_{tr} = 3$ ps, and equilibrium drift velocity ($\sim 1 \times 10^7$ cm/s) for $t_{tr} > 3$ ps. Hole motion is approximated by one third of the electron velocity at any given $t_{tr} \geq t_{onset}$ resulting in velocities lower than those reported for GaAs[17].

The integral of curves in Fig 3 give the carriers (N_e, N_h for electrons and holes respectively) generated per period ($T \simeq 2.83$ fs) of the 850 nm source with $P_0 = 60$ mW. For the parameters of Fig 2, $\sim 98\%$ of incident power is

absorbed in LT-GaAs layer while n_{tr} has peaks at $t_{tr} \approx 65$ and 70 fs for electrons and holes respectively (solid red and dotted blue curves). Such a sharp peak followed by several satellite peaks and a long tail of the n_{tr} distribution can be understood from the fact that most of the carriers are generated close to the electrodes in the near field enhancement regions where the static fields are also strong. The satellite peaks result from periodicity of the electrode structure and specific choice of the velocity distribution. As $t_{tr} < 1$ ps for majority of carriers in Fig 3, τ is not a critical factor in determining the performance at THz frequencies. A sharp drop in n_{tr} by a factor of 2 for electrons and a factor of 3 for holes at $t_{tr} \approx t_{onset}$ is due to the lower estimate of carrier velocities for $t_{tr} > t_{onset}$ resulting from the uniform field quasiballistic distribution function[18] applied to a case where fields are inherently inhomogeneous. Although, the above choice of velocity distribution for quasiballistic motion is consistent with the fact that over a large volume fraction of the absorbing layer the static field is ~ 18 kV/cm (not shown), a rigorous calculation should include quasiballistic velocity distribution appropriate for inhomogeneous fields. This would require ensemble Monte Carlo and carrier trajectory calculations carried out simultaneously. However, above calculations are adequate for obtaining the lower limit of the THz power output because a rigorous calculation would probably produce a more uniform $n_{tr}(t_{tr})$ distribution around $t_{tr} \approx t_{onset}$ without altering the distribution for $t_{tr} < t_{onset}$ or the integral of $n_{tr}(t_{tr})$. This will further reduce the number of carriers in the long tail of the n_{tr} distribution.

Based on above $n_{tr}(t_{tr})$ distributions, the number of electrons captured in the metal electrodes at time t will be

$$n_{cap}^e(t) = \int_{t_c=0}^{t_c=t} n_{gen}^e(t_c) n_{tr}^e(t - t_c) e^{-(t-t_c)/\tau_e} dt_c, \quad (2)$$

where $n_{gen}^e(t) = \frac{N_e c}{\lambda_0} [1 + \cos(2\pi f t)]$ is the number of electrons generated in LT-GaAs layer per second and t_c is the carrier creation time. Similar expressions can be written for number of holes captured $n_{cap}^h(t)$ and the electrons/holes available for conduction in the photomixer $n_{avl}^e(t)$, $n_{avl}^h(t)$. In the calculation of n_{cap} , n_{avl} , $i_p(t) = e(n_{cap}^e(t) + n_{cap}^h(t))$ (e is electron charge), and P_f , we set $R_L = 72 \Omega$, $\tau = 2\tau_e = 2\tau_h/3$ [14], and varied τ in the 0.5 to 6 ps range. For the parameters of Fig 2, the steady state electron density \bar{n} obtained from the dc value of $n_{avl}^e(t)$ for $\tau = 4$ ps is $\sim 6 \times 10^{15} \text{ cm}^{-3}$ (at $P_0 = 60$ mW) with holes 1.5 times more numerous than electrons. We estimated that dipole fields arising from this space charge are negligible ($< 2.5\%$) in comparison to strong fields (Fig 2b) present in the photomixer.

We have carried out calculations for over 70 configurations by systematically varying D , L_x , L_y , d , z_i , p , w , l_1 , l_2 , i , polarization of

the lasers (E_x or E_y), orientation of interdigitated lines in different layers, and DBR parameters. Fig 4 shows the P_f values obtained from Eq 1 and 2 for some of the configurations in the 0.1 to 10 THz range. The data shows that $P_f \propto f^{-2.77}$ in the 0.5 to 6.5 THz range in contrast to f^{-4} roll-off of P_f for a conventional photomixer[14]. A recent nip-nip photomixer concept is shown to have f^{-2} roll-off for $f < 1.5$ THz[12]. Therefore, the design of Fig 1 exploiting SPPs offers significant improvement over the existing photomixer designs. Based on 3D FD computation of steady-state heat equation with appropriate thermal boundary conditions for the device parameters of Fig 2 ($P_0 = 60$ mW, $V_b = \pm 1$ V), internal temperature (T_i) of the device is estimated to be ~ 200 K above the substrate temperature requiring substantial cooling (to 77 K) when P_0 is high. Thermal conductivity (k) of various DBR layers and that of LT-GaAs are approximated by assigning $k_{\parallel}^{\text{LT-GaAs}} = 46 \text{ Wm}^{-1}\text{K}^{-1}$ and $k_{\perp}^{\text{LT-GaAs}} = k_{\parallel}^{\text{DBR}} = k_{\perp}^{\text{DBR}} = 10 \text{ Wm}^{-1}\text{K}^{-1}$, where k_{\parallel}/k_{\perp} are in-plane/out-of-plane conductivities. This internal heating therefore limits P_0 to ~ 60 mW. However, the structure of Fig 1b, which is equivalent to two capacitors in series coupled to the antenna or transmission line, offers an alternative. If it is excited by TEM₀₁ mode lasers with total power $P_0 = 120$ mW as shown, the output can be increased to $2P_f$ (of Fig 4) without worsening T_i or \bar{n} . To demonstrate the applicability of this method to other semiconductor materials, similar calculations are carried out for two more photomixers based on Be doped $\text{In}_{1-x}\text{Ga}_x\text{As}$ and GaN optimized for operation at $\lambda_0 = 1550$ and 343 nm respectively. Both structures show strong near field enhancement arising from SPPs similar to Fig 2a and further work is underway to calculate the device efficiencies. Author wishes to thank John Goodkind for introducing him to the fascinating subject of Auston switches.

* Electronic address: manyamp@gmail.com

- [1] T. W. Ebbesen, H. J. Lezec, H. F. Ghaemi, T. Thio, and P. A. Wolff, Nature **391**, 667 (1998).
- [2] W. L. Barnes, A. Dereux, and T. W. Ebbesen, Nature **424**, 824 (2003).
- [3] S. I. Bozhevolnyi, V. S. Volkov, E. Devaux, and T. W. Ebbesen, Phys. Rev. Lett. **95**, 046802 (2005).
- [4] H. Furukawa and S. Kawata, Opt. Commun. **148**, 221 (1998).
- [5] J. P. Harbison, D. M. Hwang, J. Levkoff, and G. E. Derkits Jr., Appl. Phys. Lett. **47**, 1187 (1985).
- [6] J. E. Bjarnason, et al., Appl. Phys. Lett. **85**, 3983 (2004).
- [7] D. M. Mittleman, R. H. Jacobsen, and M. C. Nuss, IEEE J. Select. Top. Quant. Electron. **2**, 679 (1996).
- [8] J. C. Pearson et al., Proc. SPIE **5498**, 486 (2004).
- [9] R. M. Woodward, V. P. Wallace, D. D. Arnone, E. H. Linfield, and M. Pepper, J. Biol. Phys. **29**, 257 (2003).

- [10] K. Kawase, Y. Ogawa, and Y. Watanabe, *Opt. Express* **11**, 2549 (2003).
- [11] H. Ito, F. Nakajima, T. Furuta, and T. Ishibashi, *Semicond. Sci. Technol.* **20**, S191 (2005).
- [12] G. H. Dohler et al., *Semicond. Sci. Technol.* **20**, S178 (2005).
- [13] R. Kohler et al., *Nature* **417**, 156 (2002).
- [14] E. Brown, *Appl. Phys. Lett.* **75**, 769 (1999).
- [15] M. Suzuki and M. F. Tonouchi, *Appl. Phys. Lett.* **86**, 051104-3 (2005).
- [16] M. Betz et al., *Semicond. Sci. Technol.* **19**, S167 (2004).
- [17] Y. Awano, Y. Tagawa, and M. Shima, *IEEE/Cornell Conference on Advanced Concepts in High Speed Semiconductor Devices and Circuits, Proceedings.*, 408 (1995).
- [18] A. Reklaitis, A. Krotkus and G. Grigaliunaite, *Semicond. Sci. Technol.* **14**, 945 (1999).
- [19] J. L. Thobel, L. Baudry, A. Cappy, P. Bourel, and R. Fauquembergue, *Appl. Phys. Lett.* **56**, 346 (1990).
- [20] B. E. Foutz, L. F. Eastman, U. V. Bhapkar, and M. S. Shur, *Appl. Phys. Lett.* **70**, 2849 (1997).
- [21] M. Wraback, H. Shen, S. Rudin, and E. Bellotti, *Phys. Stat. Sol. (B)* **234**, 810 (2002).
- [22] K. S. Yee, *IEEE Trans. Ant. Prop.* **AP-14**, 302 (1966).
- [23] A. Taflov and S. C. Hagness, *Computational Electrodynamics - The Finite Difference Time-Domain Method*(Artech House Publishers, Norwood, MA).
- [24] Y. Park et al., *Appl. Phys. Lett.* **82**, 2770 (2003).
- [25] O. S. Heavens, *Rep. Prog. Phys.* **23**, 1 (1960).
- [26] J. B. Judkins and R. W. Ziolkowski, *J. Opt. Soc. Am. A* **12**, 1974 (1995).
- [27] *Numerical Techniques in Electromagnetics* 2nd Ed. by M. N. O. Sadiku, CRC Press, Washington D.C., USA.
- [28] L. K. Elbaum, K. Ahn, J. H. Souk, C. Y. Ting, and L. A. Nesbit, *J. Vac. Sci. Technol. A* **4**, 3106 (1986).